

ARTICLE

Open Access

TM4SF5-mediated CD44v8-10 splicing variant promotes survival of type II alveolar epithelial cells during idiopathic pulmonary fibrosis

Ji Eon Kim¹, Hye-Jin Kim¹, Jae Woo Jung^{1,2}, Dae-Geun Song^{1,3}, Dasomi Park¹, Haesong Lee¹, Hyejin Um¹, Jinsoo Park¹, Seo Hee Nam¹, Moonjae Cho⁴ and Jung Weon Lee^{1,2}

Abstract

Reactive oxygen species (ROS) regulate cell fate, although signaling molecules that regulate ROS hormesis remain unclear. Here we show that transmembrane 4 L six family member 5 (TM4SF5) in lung epithelial cells induced the alternatively spliced CD44v8-10 variant via an inverse ZEB2/epithelial splicing regulatory proteins (ESRPs) linkage. TM4SF5 formed complexes with the cystine/glutamate antiporter system via TM4SF5- and CD44v8-10-dependent CD98hc plasma-membrane enrichment. Dynamic TM4SF5 binding to CD98hc required CD44v8-10 under ROS-generating inflammatory conditions. TM4SF5 and CD44v8-10 upregulated cystine/glutamate antiporter activity and intracellular glutathione levels, leading to ROS modulation for cell survival. *Tm4sf5*-null mice exhibited attenuated bleomycin-induced pulmonary fibrosis with lower CD44v8-10 and ESRPs levels than wild-type mice. Primary mouse alveolar epithelial cells (AECs) revealed type II AECs (AECII), but not type I, to adapt the TM4SF5-mediated characteristics, suggesting TM4SF5-mediated AECII survival following AECI injury during idiopathic pulmonary fibrosis (IPF). Thus, the TM4SF5-mediated CD44v8-10 splice variant could be targeted against IPF.

Introduction

Idiopathic pulmonary fibrosis (IPF) is a chronic interstitial lung disease with fibrotic remodeling leading to respiratory failure. IPF is characterized by abnormal cell fates, enriched extracellular matrix (ECM), elevated levels of reactive oxygen species (ROS), and eventual destruction of lung architecture¹. However, it is still unclear how these characteristics correlate with molecular regulation. Damage to the alveolar epithelium by genetic and environmental factors leads to activation of myofibroblasts expressing α -smooth muscle actin (α -SMA) and subsequent secretion and deposition of ECM components characteristic of IPF development². Molecular links

between injury and dysfunction of alveolar epithelium, and activation of myofibroblasts, include the profibrotic cytokine TGF β 1^{3,4} and ROS generated by nicotinamide adenine dinucleotide phosphate-reduced (NADPH) oxidase (NOX)⁵. ROS can also activate TGF β 1 signaling to promote fibrosis⁶. ROS generated from infectious disease, trauma, toxins, drugs, and radiation directly and indirectly contributes to fibrosis via inflammatory responses. Cytokines and growth factors produced by inflammation also contribute to excessive ROS generation⁵. Intracellular levels of ROS can either promote or inhibit cell death in a hormetic manner⁷. Although ROS accumulation in lung epithelial cells is critical for IPF development, the molecular mechanism of ROS modulation in lung epithelia remains unelucidated.

Elevated TGF β 1 signaling and ROS accumulation in an inflammatory environment following epithelial injury leads to aberrant ECM production and deposition⁸. Aberrant ECM synthesis and deposition involved in IPF

Correspondence: Jung Weon Lee (jwl@snu.ac.kr)

¹Department of Pharmacy, Research Institute of Pharmaceutical Sciences, College of Pharmacy, Seoul National University, Seoul 08826, Republic of Korea
²Interdisciplinary Program in Genetic Engineering, Seoul National University, Seoul 08826, Republic of Korea

Full list of author information is available at the end of the article.
Edited by A. Stephanou

© The Author(s) 2019



Open Access This article is licensed under a Creative Commons Attribution 4.0 International License, which permits use, sharing, adaptation, distribution and reproduction in any medium or format, as long as you give appropriate credit to the original author(s) and the source, provide a link to the Creative Commons license, and indicate if changes were made. The images or other third party material in this article are included in the article's Creative Commons license, unless indicated otherwise in a credit line to the material. If material is not included in the article's Creative Commons license and your intended use is not permitted by statutory regulation or exceeds the permitted use, you will need to obtain permission directly from the copyright holder. To view a copy of this license, visit <http://creativecommons.org/licenses/by/4.0/>.

affects cell fates of alveolar epithelial cells (AECs); type I AECs (AECI) undergo apoptosis, and type II AECs (AECII) are hyperplastic and hypertrophic during IPF⁹. AECII function as facultative stem cells of alveolar epithelium leading to AECI regeneration in response to epithelial injury during IPF¹⁰. Pathological inflammation along with intracellular ROS accumulation is critically involved in pulmonary fibrosis¹¹. Therefore, the identification of a hormetic regulator of intracellular ROS levels in response to pathological inflammation is essential for prevention and treatment of inflammatory diseases such as fibrosis.

Transmembrane 4 L six family member 5 (TM4SF5) is an *N*-glycosylated membrane protein with four transmembrane domains that forms massive protein complexes on the cell surface at TM4SF5-enriched microdomains (T₅ERMs)¹² like tetraspanins. TM4SF5 interacts with the EGF receptor and integrin $\alpha 5$ ¹³ and binds to CD151 and CD63 tetraspanins¹⁴. TM4SF5 expression is associated with liver fibrosis in CCl₄-treated animals¹⁵ and hepatic cancer¹⁶. Therefore, TM4SF5 has potential roles in the development of pathological conditions in response to chronic inflammation. In addition, further investigation is warranted to determine if TM4SF5 modulates intracellular ROS during pulmonary fibrosis.

This study examined TM4SF5 function in the regulation of intracellular ROS during IPF development. We hypothesized that TM4SF5 could be a signaling-hub molecule in T₅ERMs¹², leading to dynamic activation of the xc⁻ system consisting of CD98hc and xCT (SLC7A11), a cystine/glutamate antiporter, in response to ROS-generating stimuli. TM4SF5 could therefore control intracellular ROS levels and AEC fates during IPF. We found that increased TM4SF5 expression in lung epithelial cells, but not hepatocytes, induced a CD44v8-10 alternatively spliced variant and formed complexes with the xc⁻ system via ROS-induced membrane localization of CD98hc, depending on TM4SF5-induced CD44v8-10. This led to hormetic intracellular glutathione (GSH) and ROS modulation. Furthermore, TM4SF5-mediated effects on ROS regulation and fibrotic phenotypes were observed in primary AECII from bleomycin-treated wild-type mice, but not from *Tm4sf5*-knockout mice. Thus, TM4SF5 and CD44v8-10 could be promising therapeutic targets for the prevention and treatment of IPF.

Results

Proteomic analysis for TM4SF5-binding proteins in hepatic epithelial cells revealed CD44 interaction with TM4SF5¹⁷. Because there are different alternatively spliced variants of CD44¹⁸, we examined if TM4SF5 exhibited relationships with specific CD44 variant forms. We first discovered that mRNA levels of *CD44* variants were minimally expressed in hepatic epithelial cells, in

particular a CD44 variant form, *CD44v8-10*, with exons 13–15, in addition to a standard form, *CD44s*, that has exons 1–5 and 16–20 (Fig. S1A). In addition, ectopic TM4SF5 expression in SNU761 hepatocytes failed to result in CD44 variant mRNA expression profile changes (Fig. S1B). However, TM4SF5-positive lung epithelial cells positively correlated with *CD44v8-10* mRNA expression (Fig. 1a). Ectopic TM4SF5 expression in lung epithelial cells increased *CD44v8-10* mRNA levels, decreased *CD44s* mRNA levels, and increased CD44v8-10 protein levels (Fig. 1b, c). Using a splicing luciferase reporter system, we found that TM4SF5 suppression inhibited splicing processes of the intron-containing construct, but not the construct lacking introns (Fig. S1C). Although total *CD44* mRNA levels were not affected by TM4SF5 expression (Fig. S1D, left), suppression of TM4SF5 increased *CD44s* mRNA levels and simultaneously reduced *CD44v8-10* mRNA (Fig. 1d) and protein levels (Fig. 1e). These results suggest a TM4SF5-dependent shift in expression from the CD44s to CD44v8-10 form.

We next examined molecules in lung epithelial cells that could be involved in TM4SF5-mediated *CD44v8-10* mRNA elevation. Among diverse alternative splicing mRNA regulators, *ESRP1* and *ESRP2* positively correlated with *TM4SF5* mRNA levels (Fig. 1f). Exogenous expression or suppression of TM4SF5 led to enhanced or reduced *ESRP1* mRNA levels, respectively (Fig. 1g). Concomitantly, TM4SF5 induced *CD44v8-10* mRNA (Fig. S1D, right). Suppression of *ESRP1* reduced CD44v8-10, but increased CD44s protein levels (Fig. S1E); the opposite effect was observed with *ESRP1* overexpression (Fig. 1h). Upon *ESRP1* suppression, TM4SF5-overexpression-induced CD44v8-10 protein levels were reduced and CD44s levels were restored (Fig. 1i). This correlation between *ESRP1* and *CD44v8-10* was further inversely linked to *ZEB2* mRNA levels, although *ZEB2* mRNA levels did not affect *TM4SF5* and total *CD44* mRNA levels. These indicated that *ZEB2* is downstream of TM4SF5 but upstream of *ESRP1* and CD44v8-10 (Fig. 1j). In addition, suppression of *TM4SF5* in lung epithelial cells increased *ZEB2* and decreased *ESRP1* and *ESRP2* mRNA levels without affecting other splicing regulators (Fig. 1k and S1F). Meanwhile, *ESRP1* mRNA levels were not significant in hepatocytes, but more obvious in lung epithelial cells (Fig. S1G). Correspondingly, certain lung cell lines from the Cancer Cell Line Encyclopedia (CCLE) that highly express TM4SF5 exhibited a positive correlation with *ESRP1/2* expression and negative correlation with *ZEB2* expression (Fig. 1l). These data thus suggest that TM4SF5/*ESRP1*-mediated splicing variant CD44v8-10 is mechanistically involved in lung cell homeostasis following TM4SF5-mediated *ZEB2* suppression.

Next, we examined how TM4SF5-mediated CD44v8-10 expression affected lung cell homeostasis. Because we

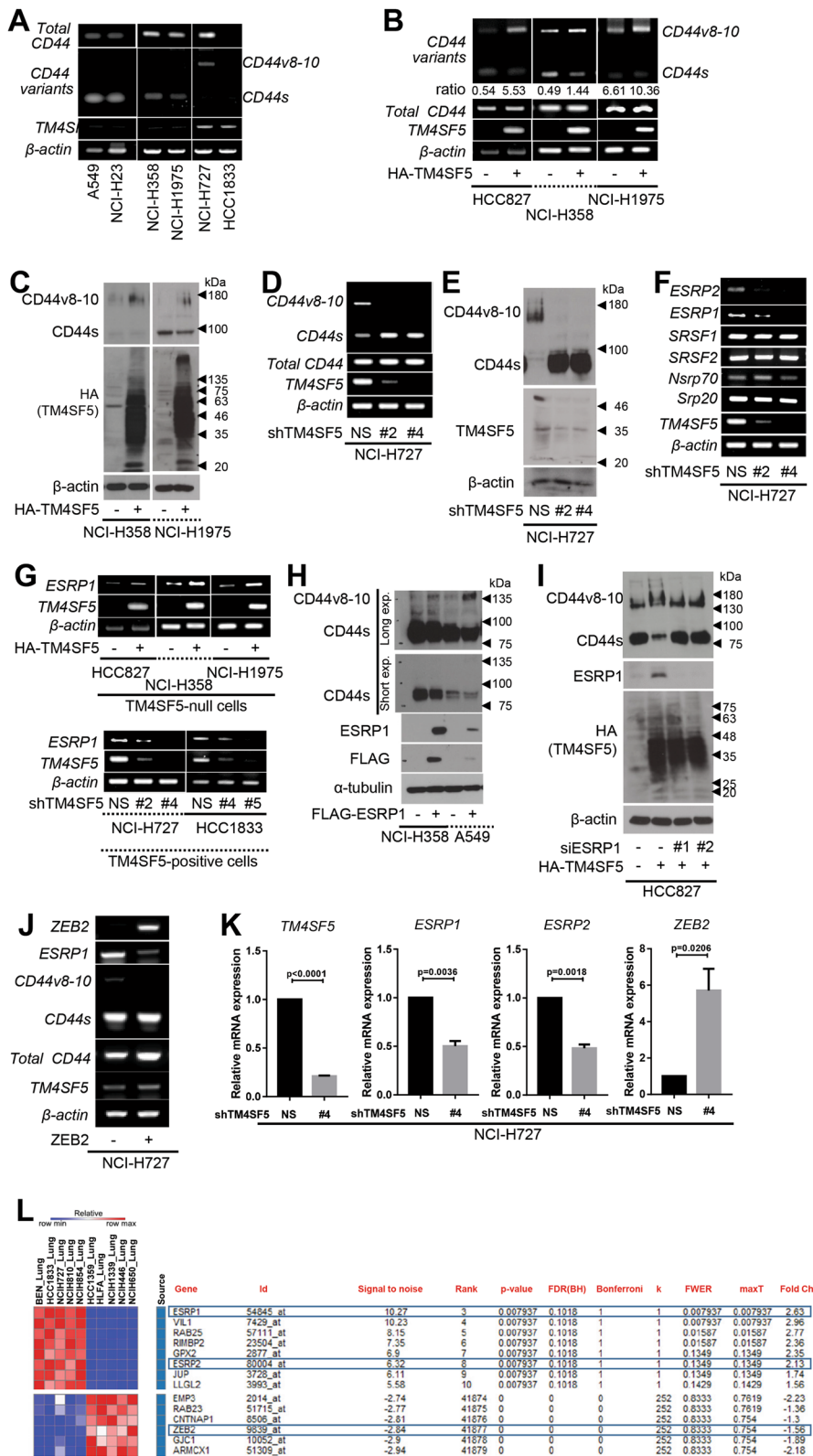


Fig. 1 (See legend on next page.)

(see figure on previous page)

Fig. 1 TM4SF5 expression induced alternative splicing variant CD44v8-10 depending on ZEB2 and ESRPs. **a–c** Different lung epithelial cells transduced without or with HA-TM4SF5 retrovirus were processed for RT-PCR (**a, b**) or western blot analysis (**c**). **d–g** Diverse lung epithelial cells transduced with shRNA for a control (NS) or TM4SF5 sequences (shTM4SF5, #2 or #4, Table 1), or transduced with control (–) or HA-TM4SF5 plasmid-containing retrovirus (+) were processed for RT-PCR (**d, f, and g**) or western blot analysis (**e**). **h–j** Lung cells transduced with control (–) or FLAG-ESRP1 (**h**), HA-TM4SF5 retrovirus, siRNA (–) or siESRP1 (#1 or #2 sequence, Table 1) (**i**), and control plasmid (–) or ZEB2 plasmid-containing retrovirus were processed for western blot analysis (**h, i**) or RT-PCR (**j**). **k** NCI-H727 cells were transduced with control (NS) or shTM4SF5-containing lentivirus (#4 sequence, Table 1) prior to qRT-PCR analysis. The *p* values were calculated by two-tailed unpaired Student's *t*-test. *P* values <0.05 were considered statistically significant. **l** Analysis of TM4SF5-positive lung cell lines from the Cancer Cell Line Encyclopedia (CCLE) for expression levels of the indicated (blue boxed) molecules. Data shown represent three independent experiments. See also Figure S1

previously demonstrated that CD44 binds TM4SF5, resulting in stem cell properties and metastasis of TM4SF5-positive liver cancer cells¹⁷, we hypothesized that CD44s and CD44v8-10 differentially bind to TM4SF5. However, no differential or competitive TM4SF5 binding of the CD44 forms was found (Fig. 2a, b, and S2A). We then investigated TM4SF5- and CD44-binding proteins via proteomic approaches and found 11 common binding proteins, including CD98hc (Fig. 2c and Table S1). TM4SF5 co-precipitated CD98hc (a heavy chain of CD98) and xCT (i.e., SLC7A11; a light chain for CD98) (Fig. 2d, e), which are the two components of the xc⁻ system, a cystine/glutamate antiporter¹⁹. Among the transmembrane 4 L six family member isoforms, TM4SF5 bound CD98hc more than TM4SF1 or TM4SF4 did (Fig. S2B). TM4SF5 binding to CD98hc was abolished by *N*-glycosylation-deficiency in TM4SF5 (Fig. S2C). The TM4SF5 C-terminal half (amino acids 91–197) bound CD98hc (Fig. S2D), which was abolished by deletion of the fourth transmembrane domain (TM4) and cytosolic C-terminus (Δ TM4/C). Deletion of the TM4SF5 cytosolic C-terminus led to weakened xCT binding compared with wild-type TM4SF5 (Fig. S2E). These data indicate that TM4SF5 associates with CD98hc mostly through TM4SF5 TM4. Furthermore, another light chain paired with CD98hc, SLC7A5, also bound TM4SF5 (Fig. S2F), indicating that TM4SF5 has a binding capacity for the xc⁻ system.

Next, we hypothesized that ROS-generating cellular events regulate binding between TM4SF5 and the xc⁻ cystine/glutamate antiporter system. Therefore, we used tumor necrosis factor- α (TNF- α), a potent, pleiotropic, pro-inflammatory cytokine that leads to ROS generation in response to cellular injury and inflammation²⁰. TNF- α treatment led to transient binding of TM4SF5 with CD98hc, but more stable binding with xCT (SLC7A11) (Fig. 2f, g). In addition, serum starvation increased ROS levels, which were significantly reduced by TM4SF5 expression; this effect was augmented by culture with 10% serum-containing medium (Fig. 2h). Serum deprivation of lung epithelial cells led to a more serum deficiency-sensitive (or -responsive) association of TM4SF5 with CD98hc than with xCT (Fig. 2i), which was abolished by

treatment with *N*-acetyl-L-cysteine (NAC), a ROS scavenger (Fig. 2j). CD44-null cells showed protein interactions less responsive to serum deprivation or TNF- α treatment (Fig. S2G and S2H). Also, NOX2/NOX4 overexpression, known ROS generators⁵, promoted TM4SF5-CD98hc binding (Fig. S2I). TM4SF5 binding to CD98hc and xCT was abolished in the presence of a specific TM4SF5 inhibitor, TSAHC [4'-(*p*-toluenesulfonylamido)-4-hydroxychalcone]²¹ (Fig. 2k). Furthermore, an Ala mutation of Ser301 (that exists only in CD44v8-10 but not in CD44s) abolished TNF- α -induced TM4SF5 binding to CD98hc, but not significantly to xCT (Fig. 2l), implicating the importance of the CD44v8-10 variant in TM4SF5-CD98hc complex formation. Thus, these data support a dynamic TM4SF5-CD98hc interaction under ROS-generating conditions that critically involves CD44v8-10.

We next examined how TM4SF5 modulated intracellular ROS levels in AECs. NOX2/NOX4 overexpression, serum deprivation, and TNF- α treatment increased ROS levels that were partially restored to baseline levels by TM4SF5 overexpression (Fig. 3a–d and Fig. S3A–C). Furthermore, mouse embryonic fibroblasts (MEFs) isolated from wild-type (*Tm4sf5*^{+/+}), heterozygous (*Tm4sf5*^{-/+}), and homozygous (*Tm4sf5*^{-/-}) mice exhibited a gradual increase in ROS levels with *Tm4sf5* gene knockout (Fig. 3e). In addition, TM4SF5 expression decreased ROS levels even with TNF- α treatment, and this effect was reversed by TSAHC pharmacological inhibition of TM4SF5 (Fig. 3f). Furthermore, TM4SF5 overexpression decreased ROS levels even with NOX2/NOX4 overexpression; however, this effect was blocked by CD44v8-10 suppression (Fig. 3g). Thus, intracellular ROS modulation was dependent on TM4SF5 expression. Moreover, TM4SF5 suppression-mediated cell death was partially rescued by CD44v8-10 overexpression (Fig. 3h). Likewise, TM4SF5 overexpression minimized cell death and increased cell survival signaling (i.e., pS⁴⁷³Akt) in response to H₂O₂ treatment (Fig. S3D and S3E). Meanwhile, TM4SF5 suppression in NCI-H727 cells or overexpression in NCI-H358 cells did not alter the superoxide levels produced by mitochondria following TNF- α treatment (Fig. 3i). Taken together, these data indicate that TM4SF5-mediated expression of the CD44v8-10 variant

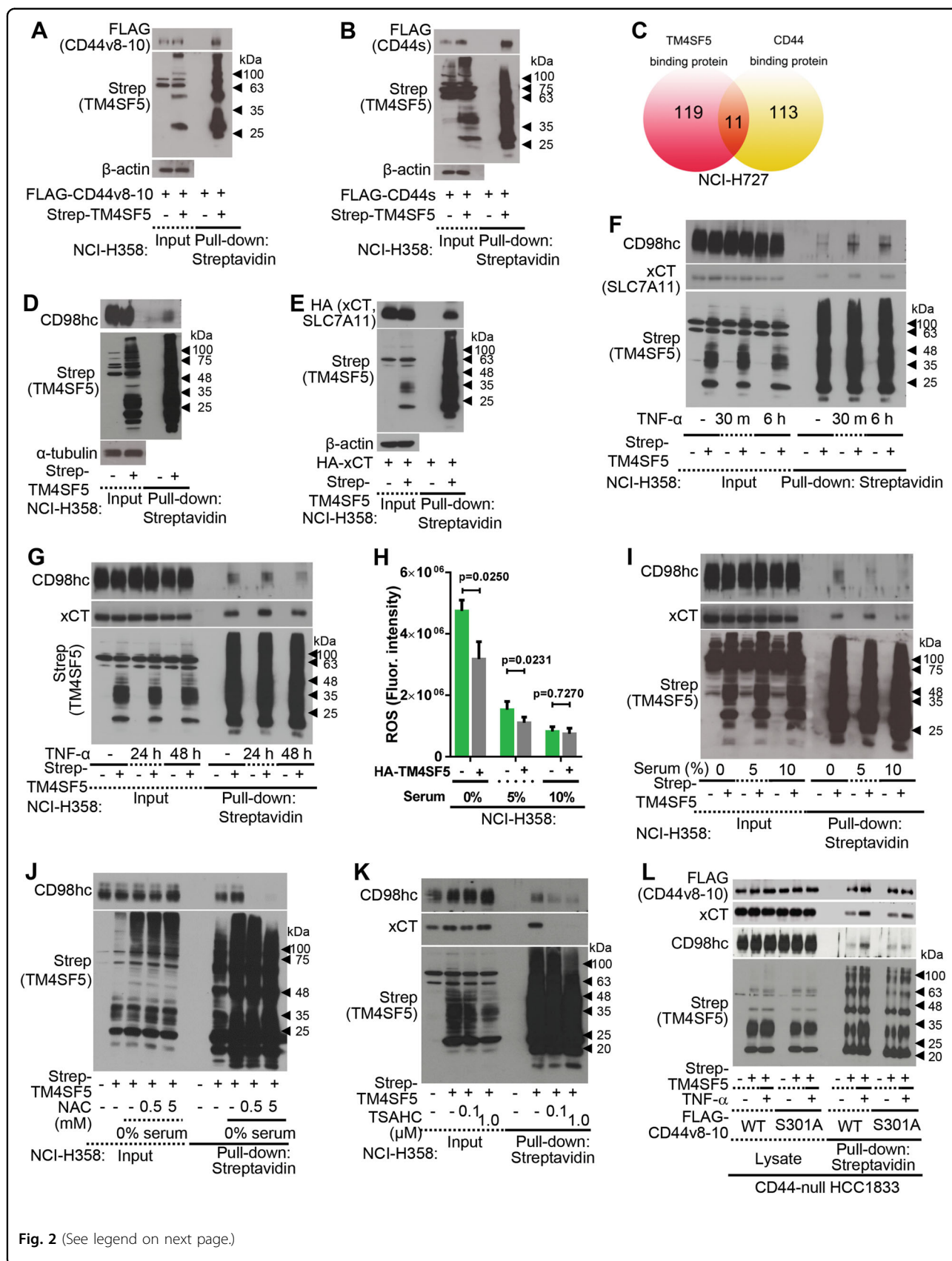


Fig. 2 (See legend on next page.)

(see figure on previous page)

Fig. 2 TM4SF5 dynamically induced CD44v8-10 protein complexes with CD98hc and xCT under ROS-generating conditions. **a, b** Cells transduced with control Strep (–) or Strep-TM4SF5 plasmid-containing retrovirus were transfected with FLAG-CD44v8-10 plasmid before preparation of whole cell lysate for pull-down with streptavidin-agarose beads and immunoblot analysis. **c** A schematic showing the quantity of molecules binding to TM4SF5 or CD44 during proteomic analysis. **d, e** Cells transduced without (**d**) or with (**e**) HA-xCT-encoding retrovirus were transfected with control Strep or Strep-TM4SF5 plasmid. Whole-cell lysates were pulled-down with streptavidin-agarose beads for western blot analysis. **f, g** Cells stably transduced with control (–) or Strep-TM4SF5-encoding retrovirus were treated with control vehicle (–) or TNF- α for the indicated times. Whole cell lysates were processed for co-precipitation analysis. **h** Cells transduced with control (–) or HA-TM4SF5 retrovirus were kept in different serum concentrations (0, 5, or 10%) before measurement of DCF-DA fluorescence to stain for intracellular ROS. **i, j** Cells transduced with control (–) or HA-TM4SF5 retrovirus were kept in different serum concentrations without (**i**) or with NAC treatment (**j**). Whole-cell lysates were processed for co-precipitation analysis. **k** Cells transfected without (–) or with Strep-TM4SF5 (+) were treated with vehicle DMSO (–) or TSAHC for 2 h. Whole-cell lysates were processed for co-precipitation analysis. **l** Cells were transfected with control (–) or Strep-TM4SF5 (+) together with wild-type (WT) or S301A mutant FLAG-CD44v8-10 plasmids, prior to TNF- α treatment (2 ng/ml) for 6 h. Whole-cell lysates were processed for co-precipitation analysis. *P* values were calculated by two-tailed, unpaired Student's *t*-test. *P* values <0.05 were considered statistically significant. Data represent three isolated experiments. See also Figure S2

exerts cellular protection against cytosolic ROS-mediated cytotoxicity.

Next, we investigated how TM4SF5-related molecules regulated the xc[–] systems for intracellular ROS modulation. We first examined if the TM4SF5 modified GSH levels. TM4SF5 substantially increased intracellular GSH levels compared with TM4SF1 and TM4SF4 (Fig. S4A). Interestingly, unlike CD44s, overexpression of CD44v8-10 enhanced cystine uptake and intracellular GSH levels (Fig. 4a). TM4SF5 overexpression or suppression increased or decreased GSH levels, respectively, in CD44-positive lung epithelial cells, whereas CD44-null lung epithelial cells did not exhibit GSH-level changes even after TM4SF5 suppression (Fig. 4a, b). GSH levels were also downregulated by CD44v8-10 suppression (Fig. 4c). Furthermore, TM4SF5 overexpression or suppression increased or decreased cystine uptake, respectively (Fig. 4d), which is responsible for intracellular GSH levels²². A specific inhibitor against the xc[–] system, erastin, blocked TM4SF5-mediated cystine uptake (Fig. 4e), as did CD98hc suppression (Fig. 4f). TM4SF5 suppression in cells under glutamate-free culture media decreased glutamate secretion, independent of additional cystine treatment (Fig. 4g). TM4SF5-dependent secretion of glutamate might occur in response to cellular stress, because glutamate levels in whole extracts prepared from cells in a normal culture condition were comparable independent of TM4SF5 expression (Fig. S4B).

We then investigated if the xc[–] system could be stabilized by TM4SF5 and CD44v8-10, because TM4SF5 has established roles in membrane trafficking and translocation with other binding partners¹³. We showed that interaction between TM4SF5 and xCT was independent of ROS-generating stimuli, whereas between TM4SF5 and CD98hc was dynamically modulated by ROS-generating stimuli. Therefore, we analyzed TM4SF5-dependent translocation of CD98hc to the plasma membrane upon ROS generation. We demonstrated that TM4SF5 expression increased translocation of CD98hc to the

plasma membrane (–proximal) regions, which was further enhanced by TNF- α -mediated ROS generation (Fig. 4h and Fig. S5A). Suppression of CD44v8-10 reduced colocalization between TM4SF5 and CD98hc on plasma membrane (–proximal) regions (Fig. 4i and Fig. S5B). Meanwhile, membrane localization of xCT (SLC7A11; another component of the xc[–] system) in the basal or TNF- α -treated conditions did not depend on TM4SF5 expression (Fig. 4j and Fig. S5C). Thus, TM4SF5 and TM4SF5-mediated CD44v8-10 facilitated membrane localization of CD98hc upon ROS generation.

Next, we explored the physiological function of TM4SF5-mediated regulation of intracellular ROS in lung epithelial cells of mice treated with bleomycin to induce pulmonary fibrosis. We postulated that TM4SF5 and its associated molecules were critically involved in pulmonary fibrosis. Intratracheal injection of bleomycin was administrated to wild-type and *Tm4sf5*-knockout (*Tm4sf5*^{–/–}) mice to induce pulmonary fibrosis. Bleomycin treatment disrupted alveolar epithelial architecture with collagen enrichment in wild-type mice, whereas *Tm4sf5*^{–/–} mice displayed a decreased phenotype (Fig. 5a). Immunostainings for the fibrotic biomarkers α -SMA, fibronectin, and ESRP1 revealed fibrotic lungs in wild-type mice; this observation was minimized in *Tm4sf5*^{–/–} mice (Fig. 5b). Bleomycin treatment also increased hydroxyproline levels that are required for collagen crosslinks in wild-type mice, but this characteristic was not prevalent in *Tm4sf5*^{–/–} mice (Fig. 5c). *Tm4sf5*^{–/–} mice also exhibited increased survival rates after bleomycin treatment compared with wild-type (Fig. 5d). Primary AEC cultures were analyzed for biomarkers of AECI or AECII to evaluate further the AEC type involved in the TM4SF5-protective effects in response to bleomycin-induced pulmonary fibrosis (Fig. 5e). A positive correlation was observed among *Tm4sf5*, *Cd44v8-10*, and *Esrp1* mRNA expression levels and an inverse correlation was detected with *Zeb2* mRNA levels in AECII, but not AECI (Fig. 5f). Furthermore, primary

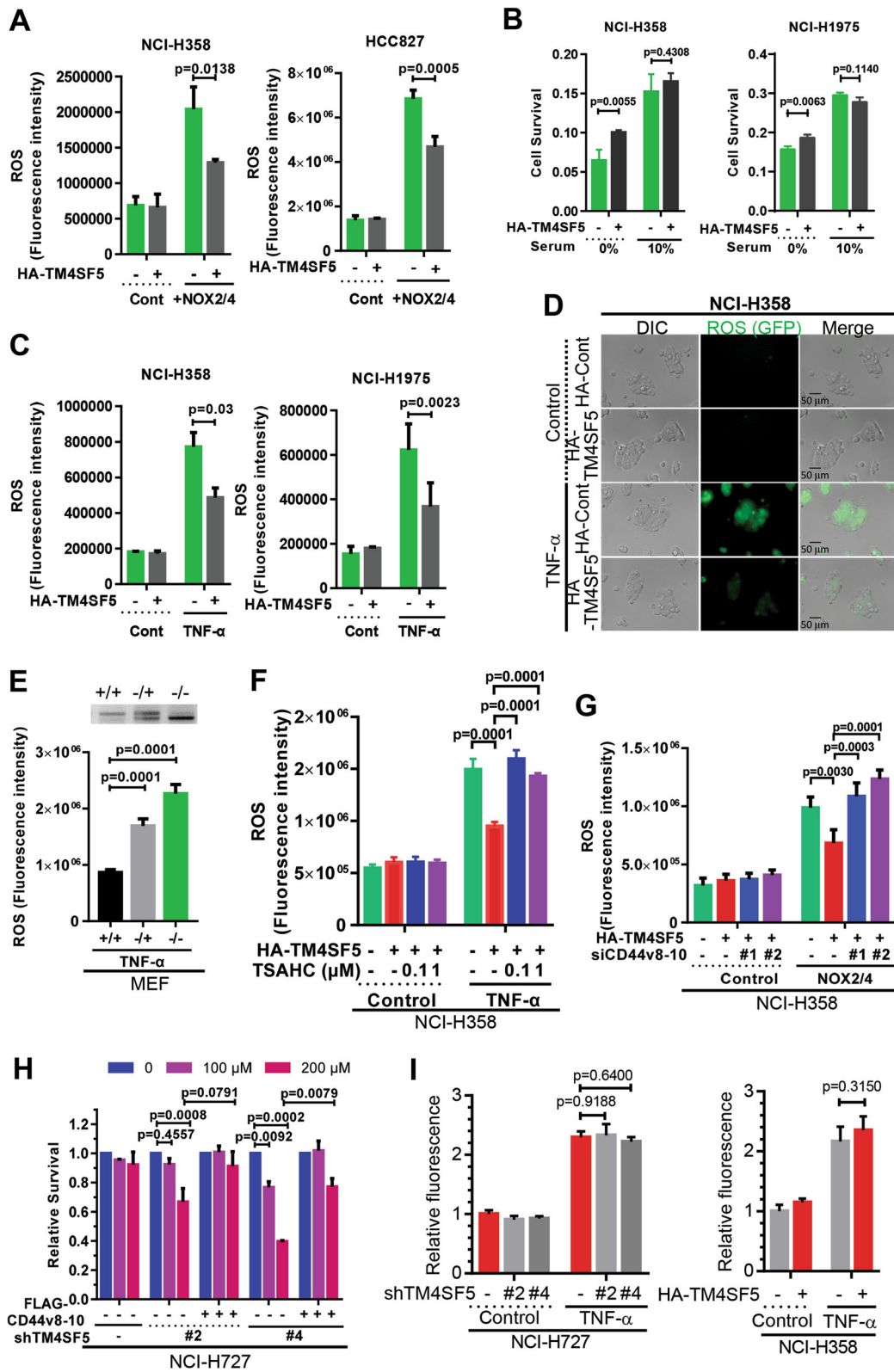


Fig. 3 (See legend on next page.)

(see figure on previous page)

Fig. 3 TM4SF5-mediated ROS modulation resulted in increased survival in epithelial cells. **a, c** Cells stably transduced with control (–) or HA-TM4SF5 plasmid-containing retrovirus were transfected with NOX2 and NOX4 plasmids (**a**) and subsequently cultured under serum starvation (**b**) or TNF- α treatment (**c**) in parallel to normal control condition (Cont) followed by DCF-DA fluorescence staining for intracellular ROS measurement. *P* values were calculated by two-tailed, unpaired Student's *t*-test. **d** Cells stably transduced with control (–) or HA-TM4SF5 retrovirus were treated with control vehicle (Control) or TNF- α , followed by fluorescence and phase-contrast imaging. **e** Mouse embryonic fibroblasts (MEFs) from wild-type (+/+), heterozygous knockout (–/+), or homozygous knockout (–/–) animals were treated with TNF- α before DCF-DA staining for ROS measurement. **f** Cells were stably transduced without (–) or with HA-TM4SF5 retrovirus with vehicle DMSO (–) or TSAHC treatment, and were concomitantly treated with TNF- α before ROS measurement. **g** Cells stably transduced without (–) or with HA-TM4SF5 retrovirus were transfected with control (–) or NOX2/NOX4 plasmids along with control (–) or siRNA against CD44v8-10 (#1 or #2 sequences, Table 1) before TNF- α treatment and ROS measurement. *P* values were calculated by two-tailed, unpaired Student's *t*-test. **h** Cells were stably transduced with control (–) or shTM4SF5-encoding (#2 or #4 sequence of TM4SF5, Table 1) lentivirus and then transfected with control (–) or FLAG-CD44v8-10 plasmid before relative cell survival measurement via MTT assay. **i** NCI-H727 cells were treated with shRNAs for a control sequence or to suppress endogenous TM4SF5 (#2 or #4), NCI-H358 cells were transfected with control (–) or HA-TM4SF5 (+) plasmids for 48 h, and they were then incubated without (Control) or with TNF- α (2 ng/ml) for 6 h before determination of MitoSOX fluorescence. The *p* values were analyzed by ANOVA with Tukey's range-test. *P* values <0.05 were considered statistically significant. Data represent three independent experiments. See also Figure S3

AECII from *Tm4sf5*^{–/–} mice showed lower *Cd44v8-10* and *Esrp1* mRNA levels compared with wild-type mice, whereas AECl did not show differential corresponding mRNA levels between wild-type and *Tm4sf5*^{–/–} mice (Fig. 5g). Likewise, CD44v8-10 and ESRP1 protein levels were higher in AECII from wild-type mice compared with *Tm4sf5*^{–/–} mice, but the standard form, CD44s, was mostly expressed in AECl without ESRP1 expression from both wild-type and *Tm4sf5*^{–/–} mice (Fig. 5h). TNF- α treatment of primary AEC resulted in decreased ROS levels in wild-type AECII, but not AECl or AEC from *Tm4sf5*^{–/–} mice (Fig. 5i), suggesting no ROS-regulatory roles of TM4SF5 in AECl. Therefore, TM4SF5 mediates hormetic levels of intracellular ROS as demonstrated by the bleomycin-induced pulmonary fibrosis model.

Discussion

This study revealed that TM4SF5 expression in lung epithelial cells induces mRNA splicing for the CD44v8-10 variant via decreased ZEB2 and, in turn, increased ESRPs. This promoted plasma membrane translocation and stabilization of CD98hc and subsequent protein complex formation with xCT to support cystine uptake and glutamate secretion for intracellular GSH-mediated ROS modulation, leading to AEC survival. However, this TM4SF5-mediated mechanism and its corresponding phenotype were observed in primary AECII, but not in AECl, in a bleomycin-induced pulmonary fibrosis animal model. Therefore, this study suggests that TM4SF5-dependent protective effects are important for IPF development (Fig. 5j), and further proposes TM4SF5 and CD44v8-10 as promising therapeutic targets against IPF.

This study revealed that CD44v8-10 variant levels depended on TM4SF5-mediated lower ZEB2 expression and, in turn, TM4SF5-dependent ESRP1/2 expression. Among diverse splicing factors, ESRP1/2 was responsible for TM4SF5-induced CD44v8-10 mRNA splicing as a

replacement for the CD44s form. It has also been observed that ESRP-regulated exons overlap exons that exhibit cell type-specific differences largely in epithelial cells compared with mesenchymal cells that alternate during the epithelial–mesenchymal transition (EMT)²³. Indeed, TM4SF5 is involved in EMT, leading to a loss of contact inhibition in liver cancer cells¹⁶ and resistance against anti-cancer drugs including paclitaxel or gefitinib^{24,25}. Therefore, as a membrane protein, TM4SF5 also triggers EMT-related stem cell properties that initiate tumor formation at low cell numbers as well as circulating tumor cell properties¹⁷. Furthermore, the TM4SF5-mediated CD44v8-10 induction occurred in primary AECII, but not AECl. Given that AECII can function as facultative stem cells in alveolar epithelium, leading to regeneration of AECl following epithelial injury¹⁰, TM4SF5 may promote AECII survival and proliferation under ROS-generating, pro-inflammatory conditions to compensate for AECl loss during IPF.

The hormetic regulation of ROS is critical for cellular homeostasis²⁶. We discovered that TM4SF5-mediated induction of the alternative splicing variant, CD44v8-10, led to intracellular ROS modulation via formation of TM4SF5/CD44v8-10/xc[–] system protein complexes. The xc[–] system consisting of CD98hc and xCT (SLC7A11) influxes cystine and effluxes glutamate, which in turn regulates intracellular GSH and ROS levels in gastric cancer cells²⁷. Here, we further elucidate the ROS-mediated regulatory circuit by the xc[–] system, depending on TM4SF5, as follows: (1) TM4SF5 specifically caused alternative splicing variant CD44v8-10 replacing CD44s via reduced ZEB2 and increased ESRP1/2 expression; (2) TM4SF5 promoted dynamic plasma membrane translocation of CD98hc in response to ROS-generating stimuli; (3) TM4SF5-CD98hc binding dynamically depended on the presence of CD44v8-10, whereas TM4SF5 constitutively bound CD44s and xCT; (4)

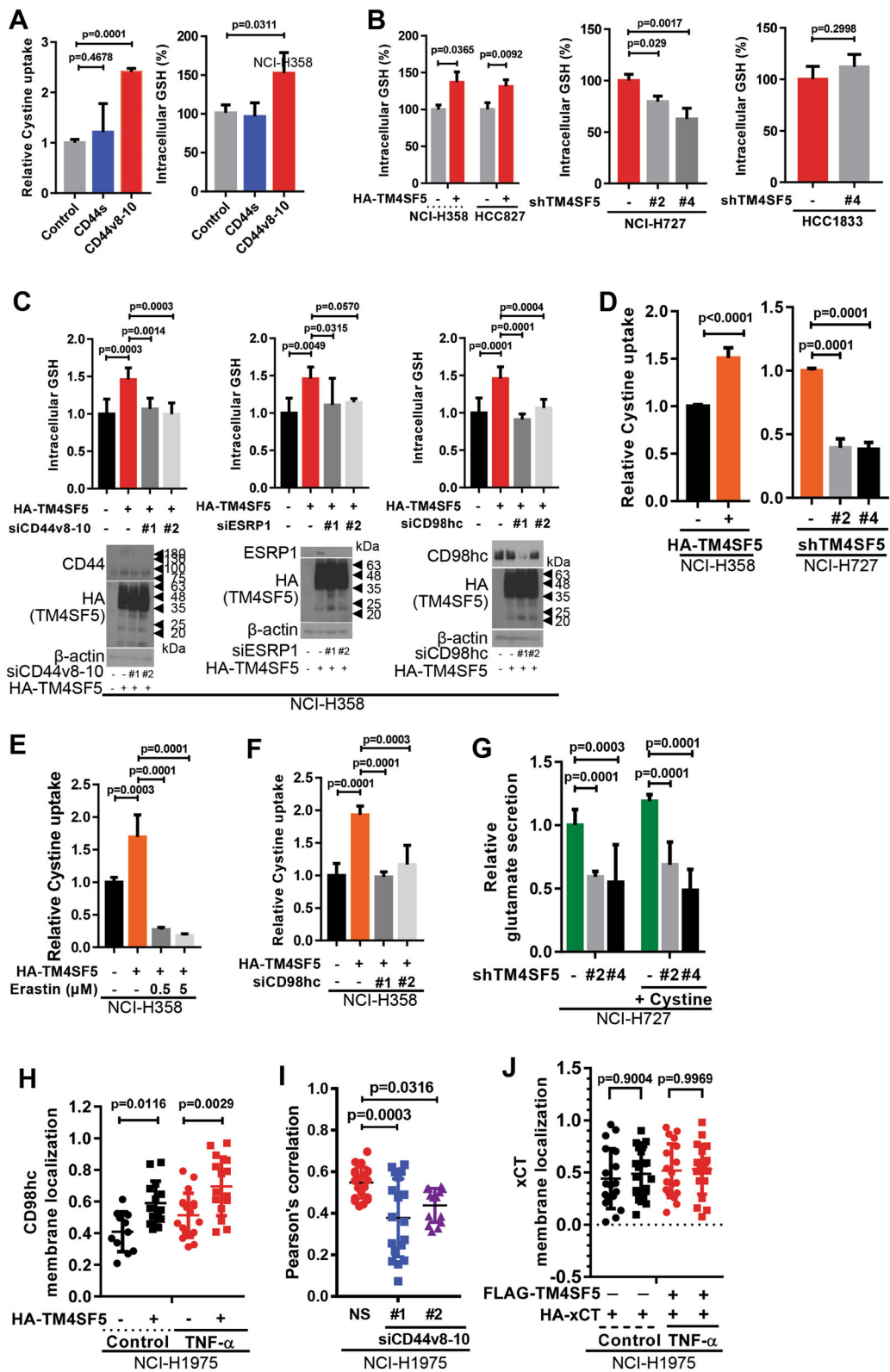


Fig. 4 (See legend on next page.)

(see figure on previous page)

Fig. 4 TM4SF5-mediated CD44v8-10 expression increased CD98hc enrichment at the plasma membrane for intracellular GSH-mediated ROS modulation. **a** Cells were transfected with control, CD44s, or CD44v8-10 plasmids, and intracellular GSH levels were measured. **b, c** Cells were transduced with the indicated retrovirus and/or lentivirus to target certain sequences of molecules (Table 1) and intracellular GSH levels were measured. Another set of cells was also processed for immunoblot analysis (bottom in **c**). **d–f** Cells transduced with different retrovirus or lentivirus without (**d, f**) or with erastin treatment (**e**) were processed for cystine uptake analysis. **g** Cells stably transduced with control (–) or shTM4SF5 (#2 or #4 sequence, Table 1) lentivirus were treated without or with cystine in glutamate-free culture media before glutamate secretion measurement. **h–j** Cells stably transduced with HA control (–) or HA-TM4SF5 retrovirus (**h**), transfected with siRNA for control (NS) or siCD44v8-10 sequence (#1 or #2, Table 1, **i**), or transfected with FLAG-TM4SF5 and HA-xCT plasmids, were treated without (**i**) or with vehicle (control) or TNF- α (**h, j**). Quantitative immunofluorescent images were analyzed for CD98hc (**h**) or xCT (**j**) localization at the plasma membrane or Pearson's values for co-localization between TM4SF5 and CD98hc at the plasma membrane (**i**). The *p* values were analyzed by ANOVA with Tukey's range-test. *P* values <0.05 were considered statistically significant. Data represent three isolated experiments. See also Figures S4 and S5

TM4SF5 and CD44v8-10 expression induced xc⁻ system activation for intracellular GSH and ROS level modulation; and (5) TM4SF5-mediated effects were observed in AECII, not AECl, during IPF. Stabilization of xCT by CD44v8-10 was exhibited in a gastric cancer model²⁷, contradictory to this study showing that CD44v8-10 was required for TM4SF5-dependent plasma membrane translocation of CD98hc. This difference could be due to different cell types, pathological states, and/or TM4SF5 expression levels. Furthermore, this study emphasizes the significance of TM4SF5-induced CD44v8-10 in the following aspects: (1) CD44v8-10 splice variant, but not CD44s, upregulated the xc⁻ system activity for cystine uptake and glutamate secretion; (2) TM4SF5-dependent plasma-membrane enrichment of CD98hc required the CD44v8-10 variant; and (3) dynamic association between TM4SF5 and CD98hc upon ROS-generating stimuli required the Ser301 residue in CD44v8-10 that does not exist in CD44s. Thus, these findings may explain why TM4SF5 expression induces alternative splicing of the CD44v8-10 variant to replace the standard CD44s form in AECII.

TM4SF5 has four transmembrane domains, similar to the tetraspanins¹². Therefore, TM4SF5 can regulate binding stability, intracellular trafficking, and signaling activity by forming massive protein-protein complexes on the cell surface at T₅ERMs²⁸. TM4SF5 expression results in acquired cancer stem cell properties via a physical association with CD44¹⁷. TM4SF5 expression is promoted by, and subsequently interacts with, CD133, a cancer cell marker²⁹. In addition to CD44 and CD133, TM4SF5 interacts with the EGF receptor and integrin α 5 for directional migration¹³. Furthermore, pro-metastatic CD151 tetraspanin binds to TM4SF5 to display a synergistic pro-metastatic role on the cell surface; however, TM4SF5 binds anti-metastatic CD63 and sequesters it from the membrane surface into lysosomes to negate its tumor-suppressive roles¹⁴. Pathological, pro-inflammatory conditions can thus selectively promote TM4SF5 binding with specific proteins at T₅ERMs in epithelial cells. The

hormetic ROS regulation appeared to be via the TM4SF5-mediated influence on the xCT system in the plasma membrane rather than ROS (especially superoxide) formation by mitochondria because TM4SF5 expression did not cause any changes in mitochondrial ROS levels. ROS-mediated cytotoxicity is involved in IPF development¹¹, and survival and hyperplasia of AECII compensates for the loss of injured AECl that is a hallmark of IPF^{1,9}. Because TM4SF5-related molecules, including ZEB2, ESRPs, and CD44v8-10, were visibly expressed in AECII, TM4SF5, and CD44v8-10 within T₅ERMs of AECII can play hyperplastic roles during IPF development. Therefore, TM4SF5-mediated hyperplasia of AECII can be targeted by an anti-TM4SF5 reagent, such as TSAHC²¹, leading to clinical benefits for IPF patients.

Materials and methods

Cell culture

A549, NCI-H23, NCI-H358, NCI-H1975, NCI-H727, and HCC1833 human lung epithelial cells and liver epithelial cells were purchased from the KCLB (Seoul National University, Seoul, South Korea). Cells were cultured in RPMI medium supplemented with 10% fetal bovine serum (FBS) (GenDepot, Barker, TX, USA), along with routine monitoring for mycoplasma contamination. For experiments requiring starvation conditions, cells were incubated overnight in culture media lacking FBS. Primary AECs were seeded into collagen-coated plates and cultured in DMEM supplemented with 10% FBS, 1 × GlutaMAX (Gibco, Waltham, MA, USA), 10 mM HEPES (Gibco), and 0.25% bovine serum albumin (GenDepot).

Viral transduction and plasmid DNA and siRNA transfection

Human TM4SF5 (NM-003963) insert was cloned into retroviral expression vector pBabe-HAII (Addgene, Cambridge, MA, USA), resulting in HA-TM4SF5. NCI-H358, H1975, and HCC827 cells were stably transduced with retrovirus expressing pBabe-HA-TM4SF5. To

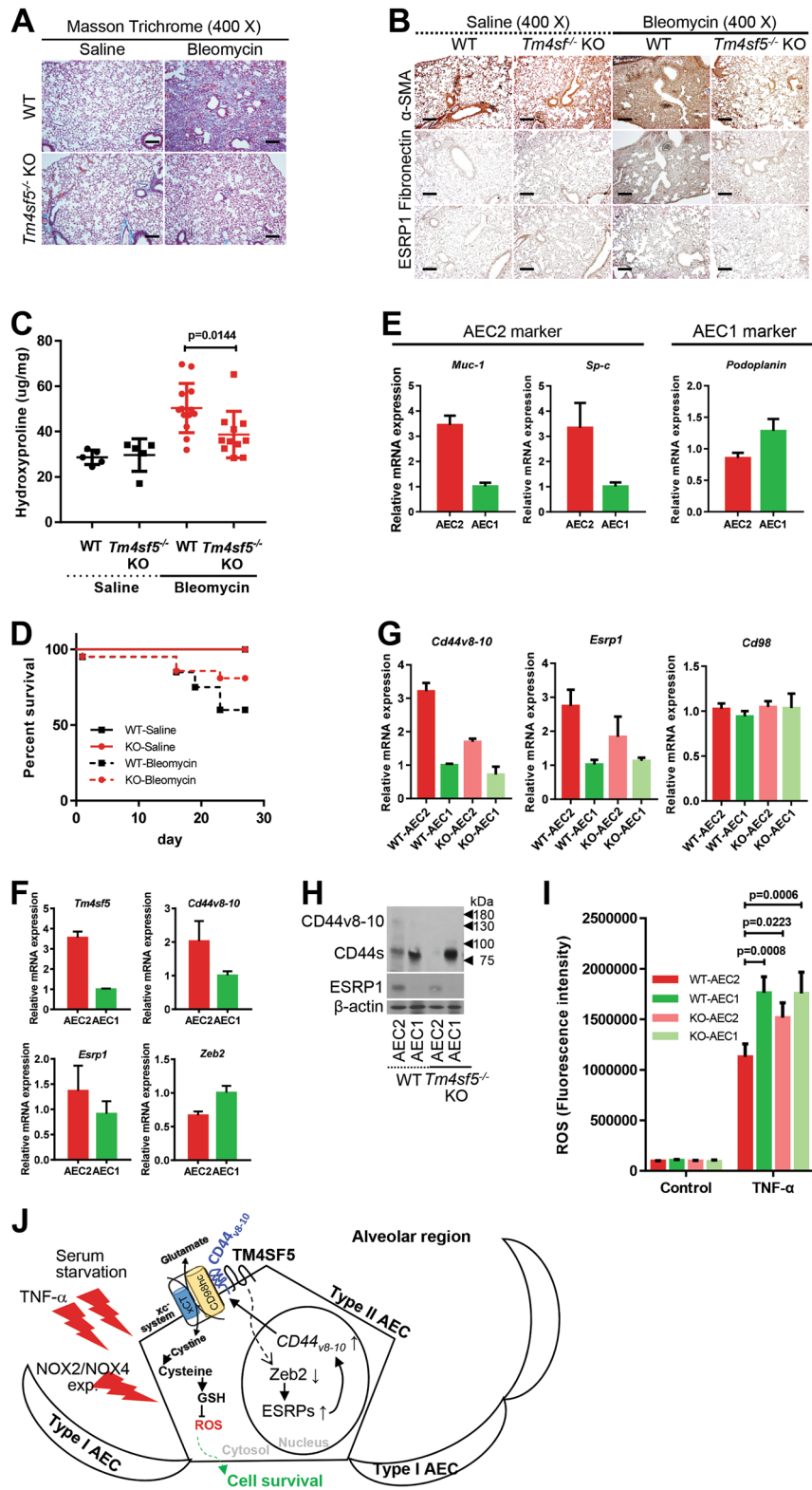


Fig. 5 (See legend on next page.)

(see figure on previous page)

Fig. 5 TM4SF5 expression was critical for AECII survival during bleomycin-induced pulmonary fibrosis. **a, b** Lung tissues from control saline or bleomycin-treated wild-type (WT) or *Tm4sf5*^{-/-}-knockout mice were analyzed for collagen levels by Masson Trichrome staining (**a**), immunohistochemistry for α -SMA and fibronectin (**b**), or hydroxyproline analysis (**c**). **d** The survival rates were plotted for WT or *Tm4sf5*^{-/-} mice treated with either control saline or bleomycin. **e, f** AECI or AECII cultures were prepared from WT mice and analyzed for AEC biomarkers (**e**) and *Tm4sf5*-related mRNAs (**f**). **g, h** Primary AECI or AECII cells were prepared from lung tissues of WT or *Tm4sf5*^{-/-} mice and processed for qRT-PCR (**g**) or western blot analyses (**h**). **i** The primary cells in (**g**) were treated with control vehicle or TNF- α , followed by DCF-DA staining for ROS. Data represent three isolated experiments. **j** The mechanistic working model. Elevated TM4SF5 expression leads to lower ZEB2 and higher splicing factor ESRP1/2 levels, leading to induction of alternative splicing variant CD44v8-10, which replaces the CD44s form. TM4SF5 and the TM4SF5-induced CD44v8-10 variant form a protein complex along with CD98hc and xCT for cystine uptake and glutamate secretion. This leads increased intracellular GSH levels for hormetic regulation of intracellular ROS levels and eventual survival or protection of AECII from cytotoxic ROS stimuli, such as serum starvation, TNF- α treatment, or NOX2/NOX4 expression

achieve *TM4SF5* knockdown, shRNAs targeting the human *TM4SF5* sequence (#2 and #4, Table 1) were cloned into lentiviral vector pLKO.1 (Addgene). NCI-H727 and HCC1833 cells were stably transduced with pLKO.1-sh*TM4SF5*-expressing lentivirus. CD44s-pBabe-puro and shCD44-pRRL constructs were purchased from Addgene. Human CD44v8-10 (NM-000610.3) and xCT (NM-014331.4) sequences were cloned from cell line NCI-H727. Plasmid cDNAs were transiently transfected into cell lines using Lipofectamine 3000 reagent (Thermo Fisher Scientific, Waltham, MA, USA) according to the manufacturer's protocol. Oligonucleotides for siRNA targeting CD44v8-10, ESRP1, or CD98hc were synthesized (Bioneer, Daejeon, South Korea), as shown in Table 1, and transfected using Lipofectamine RNAiMAX transfection reagent (Thermo Fisher Scientific) according to the manufacturer's protocols.

Western blot analysis

Cells were harvested for whole cell lysates using RIPA lysis buffer (50 mM Tris-HCl, pH 7.4, 150 mM NaCl, 0.5% Sodium deoxycholate, 0.1% SDS, and 1% NP-40) or Brij58 lysis buffer (20 mM HEPES, pH 7.4, 150 mM NaCl, 2 mM MgCl₂, 2 mM CaCl₂, and 1% Brij58) with protease inhibitor cocktails (GenDepot). The lysates were normalized and immunoblot analysis was performed using the following primary antibodies: CD44 (IM7; 1:1000 dilution), CD98hc (H-300; 1:1000 dilution), β -actin (C4; 1:1000 dilution), AKT (H-136; 1:1000 dilution), pS⁴⁷³AKT (C11; 1:1000 dilution) (Santa Cruz Biotechnology, Santa Cruz, CA, USA), ESRP1 (27H12; 1:1000 dilution; Abcam, Cambridge, UK), HA (16B12; 1:1000 dilution; Covance, Princeton, NJ, USA), StrepMAB-Classical conjugated to HRP (1:1000 dilution; IBA), FLAG (M2; 1:1000 dilution), xCT (D2M7A; 1:1000 dilution), ERKs (1:2000 dilution), and pT²⁰²pY²⁰⁴ERKs (1:5000 dilution) (Cell Signaling Technology, Danvers, MA, USA).

Immunoprecipitation assay

Cells were harvested using Brij58-containing lysis buffer. Whole-cell lysates were precipitated with Pierce

Streptavidin-Agarose (Thermo Fisher Scientific) for 4 h at 4 °C. Precipitates were washed three times with ice-cold wash buffer (20 mM HEPES, pH 7.4, 500 mM NaCl, 2 mM MgCl₂, 2 mM CaCl₂, and 1% Brij58), one time with ice-cold PBS, and then eluted in 2 \times SDS-PAGE sample buffer before immunoblot analysis.

Immunofluorescence

Cells were seeded onto glass coverslips pre-coated with fibronectin (10 μ g/ml; BD Bioscience, San Jose, CA, USA) and allowed to attach overnight. The next day, cells were fixed with ice-cold methanol and stained with the following primary antibodies: FLAG (M2; 1:300 dilution; Cell Signaling Technology), HA (16B12; 1:300 dilution; Covance), and CD98hc (H-300; 1:200 dilution; Santa Cruz Biotechnology). Immunofluorescent images were acquired at room temperature using the C2+ confocal microscope (Nikon) with a normal PMT (Nikon) and a CFI Apochromat Lambda S 60 \times NA1.49 oil immersion objective (Nikon) after excitation with 405, 488, and 561 nm laser lines. Confocal images were analyzed using NIS software (Nikon) to obtain Pearson's correlation.

Reverse transcription PCR (RT-PCR)

Total RNA was extracted from cells using Qiazol reagent (Qiagen, Hilden, Germany), according to the manufacturer's protocol. Total RNA (500 ng) was reverse transcribed into cDNA using ReverTra Ace qPCR RT master mix (Toyobo, Osaka, Japan). The primers used for PCR are listed in Table 1. Quantitative PCR (qPCR) was performed using specific primers and EvaGreen Q master mix (CosmoGenetech, Seoul, South Korea) and the CFX96 real-time system (Bio-Rad, Hercules, CA, USA). Each sample was run as triplicates. Relative fold abundance of target genes was calculated using the comparative C_t method.

ROS induction and detection

Cells were treated with TNF- α (2 ng/ml, Peprotech, Princeton, NJ, USA) for 30 min, 6 h, 24 h, or 48 h before co-precipitation processes. For intracellular ROS

Table 1 shRNA target sequence, siRNA sequence, or RT-PCR primer sequence used in this study

shRNA target sequence	Sequence (5'–3')	Species
shTM4SF5 #2	ACCATGTGTACGGGAAAATGTGC	Human
shTM4SF5 #4	CCATCTCAGCTTGCAAGTC	Human
siRNA sequence	Sequence (5'–3')	
CD44v8-10 #1	CUACUUUACUGGAAGGUUA(dTdT)	
CD44v8-10 #2	GGAAGAAGAUAAAGACCAU(dTdT)	
ESRP1 #1	CCUUCGAGGUCUCCCUAU(dTdT)	
ESRP2 #2	GCAGCAAGAUGGAACUUUAU(dTdT)	
CD98hc #1	AAUCUGAGCCUACUCGAAUC(dTdT)	
CD98hc #2	GUUCAAGAGACUUCUCGGGCU(dTdT)	
Gene	Primer sequence (5'–3')	Species
TM4SF5	FWD ACACCAACCATCTCAGCTTG	Human
TM4SF5	REV CATCTGGGTCCATTTCCGGAG	Human
CD44v8	FWD TGGACTCCAGTCATAGTATAACGC	Human
CD44v10	REV CGATTGACATTAGAGTTGGAATCTCC	Human
CD44 (total)	FWD CGGACACCATGGACAAGTTT	Human
CD44 (total)	REV GAAAGCCTTGCGAGGTCAG	Human
CD44 (variant)	FWD TCCCAGCAGACGAAGACAGTCCCTGGAT	Human
CD44 (variant)	REV CACTGGGGTGAATGTCTTGGTC	Human
ESRP1	FWD CTCTCGATATGGAGCCTCTCA	Human
ESRP1	REV CTGCACCTCCCTTGGCAATA	Human
Srp20	FWD ATGGAAGAACACTATGTGGCTG	Human
Srp20	REV GGGACGGCTGTGATTTCTCT	Human
GAPDH	FWD CCAGCCGAGCCACATCGCTC	Human
GAPDH	REV ATGAGCCCCAGCCTTCTCCAT	Human
β-actin	FWD AGAGTACGAGCTGCCTGAC	Human
β-actin	REV AGCACTGTGTGGCGTACAG	Human
ZEB2	FWD GCGATGGTCATGCAGTCA	Human
ZEB2	REV CAGGTGGCAGGTCATTTTCTT	Human
ZEB1	FWD TTACACCTTTGCATACAGAACC	Human
ZEB1	REV TTTACGATTACCCCAGACTGC	Human
SRSF1(ASF/SF2)	FWD GGAAGACGCGGTGTATGGTC	Human
SRSF1(ASF/SF2)	REV CACCTGCTTCACGCATGTG	Human
SRSF2(SC35)	FWD CCCGATGTGGAGGTATGAC	Human
SRSF2(SC35)	REV GAGACTTCGAGCGGCTGTAG	Human
NSrp70(NSRP1)	FWD GAACGTCGAGAGGACATGAGA	Human
NSrp70(NSRP1)	REV TCACGGTCAGTGAATGGTCT	Human
CD44 (total)	FWD CCGTTGGCTGCTTAGTCACAG	Mouse
CD44 (total)	REV GATGTGGATGTGCCAGGCT	Mouse

Table 1 continued

CD44 (variant)	FWD CGATGGACCGTTACCATAA	Mouse
CD44 (variant)	REV TGTCTGGTTCGCACTTG	Mouse
ESRP1	FWD CTGTGTCCCGATACGGAGC	Mouse
ESRP1	REV CTTGATCTGAAGATTGCCAGGG	Mouse
ZEB1	FWD CGCCATGAGAAGAACGAGGAC	Mouse
ZEB1	REV CTGTGAATCCGTAAGTGCTCTTT	Mouse
ZEB2	FWD AAACGTGGTGAACATGACAACG	Mouse
ZEB2	REV CTTGCAGAATCTGCCACTG	Mouse
GAPDH	FWD GTGGCAAAGTGGAGATTGTTG	Mouse
GAPDH	REV CGTTGAATTTGCCGTGAGTG	Mouse

visualization and determination, cells were incubated with 20 μM DCF-DA (Sigma-Aldrich; St. Louis, MO, USA) in RPMI for 30 min at 37 °C and washed with PBS twice. Fluorescence was visualized using fluorescent microscope (BX51TR, Olympus, Tokyo, Japan) or determined using a microplate reader (SpectraMax; Molecular Devices, San Jose, CA, USA) with an excitation wavelength at 490 nm and an emission wavelength at 520 nm. Intramitochondrial superoxide was measured using MitoSOX Red mitochondrial superoxide indicator (Invitrogen, Carlsbad, CA, USA) following the manufacturer's protocol. Cells treated with control vehicle or TNF-α (2 ng/ml for 6 h) were incubated with 2 μM MitoSOX for 10 min at 37 °C and washed with PBS twice. Fluorescence was measured using the SpectraMax microplate reader with an excitation wavelength at 510 nm and an emission wavelength at 580 nm.

Cystine uptake assay

NCI-H358 or H727 cells (200,000 cells/well) were seeded into 12-well culture plates. After 24 h, cells were washed twice with pre-warmed PBS, and then incubated for 1 h at 37 °C in amino acid-depleted RPMI media. The medium was replaced with medium containing 40 mCi/mmol L-[3,3'-¹⁴C]-Cystine (American Radiolabeled Chemicals, St. Louis, MO, USA) and incubated for 10 min at 37 °C. Cells were then washed three times with ice-cold PBS and lysed in 0.1 M NaOH. Cell lysates were added to scintillation fluid, and radioactive counts per min were obtained using a scintillation counter (Tri-Carb 2910 TR; Perkin Elmer, San Jose, CA, USA). All experiments were repeated as three independent biological replicates for each condition.

Glutamate and glutathione level assays

The Amplex Red glutamate assay kit (Thermo Fisher Scientific) or GSH-Glo glutathione assay kit (Promega,

Madison, WI, USA) were used to measure glutamate levels in medium (i.e., glutamate secretion) or for intracellular GSH levels from lysates, respectively. Assays were performed according to the manufacturer's protocols.

Cell viability assay

Cells were seeded into 96-well plates (5×10^3 cells/well) and treated with H_2O_2 (100 or 200 μM) for 24 h. Cell viability was assessed using an MTT assay. Cells were treated with 0.1 mg/ml MTT solution (Sigma-Aldrich) for 4 h at 37 °C. Crystals were solubilized using DMSO and absorbance was measured at a wavelength of 570 nm in a microplate reader (SpectraMax).

Bleomycin-induced animal pulmonary fibrosis model

Wild-type C57BL/6 mice (4 weeks old) were purchased from Orient Bio Inc. (Seongnam, South Korea). Global TM4SF5-knockout C57BL/6 mice (*Tm4sf5*^{-/-}) were generated by MacroGen (Seoul, South Korea). Briefly, base pairs of genomic TM4SF5 surrounding exon 1 were deleted using the RGEN/Cas9 genetic scissor. The genotypes of both wild-type and *Tm4sf5*^{-/-} mice were determined by PCR analysis of genomic DNA obtained from tail clippings from 3-week-old animals. Male wild-type and *Tm4sf5*^{-/-} mice at 8 weeks old were treated with either saline vehicle for the control or bleomycin (1 mg/kg, Santa Cruz Biotechnology) by intratracheal injection on day 0. Mice were sacrificed on day 28 for histological analysis and hydroxyproline assay.

Hydroxyproline assay

Total lung collagens were determined using a hydroxyproline assay kit (Sigma-Aldrich). Briefly, 10 mg lung tissue was homogenized and hydrolyzed with hydrochloric acid (HCl, ~12 M) at 120 °C for 3 h. The reaction was mixed and centrifuged at 10,000 $\times g$ for 3 min. The supernatant was transferred to a 96-well plate and 100 μl chloramine-T/oxidation buffer mixture was added to each for reaction initiation. Diluted DMAB [4-*p*-(dimethylamino) benzaldehyde, Sigma-Aldrich] reagent was added to each sample before incubation for 90 min at 60 °C. Absorbance at 560 nm was measured using a microplate reader (Zenyth 3100; Anthos Labtec Instruments; Wals/Salzburg, Austria).

Primary AECs isolation and culture

Mice at 6 weeks of age were sacrificed for primary pneumocyte isolation. A 26G cannula with a 10 ml syringe filled with cold PBS was used to puncture through the right ventricle of the heart into the lung for perfusion and complete blood removal. A 22G indwelling cannula with a 2 ml syringe was inserted into the trachea and 2 ml dispase (1 U/ml; Sigma-Aldrich) was carefully injected. The trachea was then cut, and the lung was excised and rinsed with sterilized PBS. The lung was incubated with the

injected 2 ml dispase at room temperature for 45 min. The lung tissue was transferred into a dish containing DMEM with 0.1 mg/ml DNase (Sigma-Aldrich). The lung tissue was mechanically fragmented with tweezers and incubated for 10 min at room temperature while gently rocking on a rocker. The cell suspension was filtered through nylon mesh filters with 70 and 30 μm pores. The filtrate was then transferred into 50 ml tubes, centrifuged at 160 $\times g$ for 15 min at 4 °C, and the supernatant was aspirated. The cell pellet was collected and suspended in 2 ml erythrocyte lysis buffer (150 mM NH_4Cl , 10 mM $KHCO_3$, pH 7.2, and 0.1 mM EDTA). The lysis step was quickly terminated by addition of 13 ml DMEM. The resulting solution was transferred to a 15 ml tube and centrifuged at 160 $\times g$ for 12 min at 4 °C. The cells were suspended in 3 ml primary antibody cocktail that was prepared in DMEM containing PE-coupled mouse CD11b and CD45 or APC-coupled mouse F4/80 and CD44c antibody (BioLegend, San Diego, CA, USA). For staining, the cells were incubated for 10 min in the dark at 4 °C. The cells were then washed with DMEM and centrifuged at 160 $\times g$ for 10 min at 4 °C. The cells were resuspended in 1 ml DMEM and pre-filtered through a 50 μm filter into a tube for cell sorting. Cell sorting was done by FACS (BD Bioscience, San Jose, CA, USA) using a 100 μm nozzle. Double-negative cells were collected and sorted into type I or type II AECs based on size. The cells were then centrifuged at 160 $\times g$ for 10 min at 4 °C. Cells were resuspended in either culture-medium or buffer as required for subsequent analysis.

Histology and immunohistochemistry

Lung tissues were fixed with 4% paraformaldehyde, embedded in paraffin, and sectioned at a 6- μm thickness for subsequent staining. For histological analysis, sections were stained with hematoxylin and eosin and Masson's Trichrome stain kit (Sigma-Aldrich). For immunohistochemistry analyses, sections were subjected to antigen retrieval by heating for 20 min at 100 °C in 0.01 M sodium citrate (pH 6.0) and exposure to 3% H_2O_2 before incubation with primary antibodies, including α -SMA (1A4; 1:400 dilution; Sigma-Aldrich), fibronectin (1:500 dilution; DAKO), or ESRP1 (27A12; 1:200 dilution; Abcam). Immune complexes were detected using the Vectastain Elite kit (Vector Laboratories, Burlingame, CA, USA) and 3,3'-diaminobenzidine; the sections were counterstained with hematoxylin.

Proteomic analysis for TM4SF5- and CD44-binding proteins

SNU761 cells were transiently transfected with control or Strep-tag conjugated TM4SF5 plasmid for 48 h and extracted using a Brij58-containing lysis buffer. Lysates were immunoprecipitated using streptavidin-agarose bead (Thermo Fisher Scientific) prior to separation by SDS-PAGE. After in-gel trypsin digestion of proteins, peptides

were analyzed using an LTQ XL linear trap mass spectrometer (Thermo Scientific) equipped with a nano-HPLC system (Eksigent, Dublin, CA, USA). NCI-H727 cells were transiently transfected with control or FLAG-tag conjugated CD44s or CD44v8-10 plasmids for 48 h, and then extracted using a Brij58-containing lysis buffer. Lysates were immunoprecipitated with FLAG M2 Affinity Gel (Sigma-Aldrich). After in-gel trypsin digestion, peptides were analyzed using LC-MS/MS. Tandem mass spectra were analyzed using the SEQUEST module of Proteome Discoverer (Thermo Fisher Scientific; version 1.4.1.14) and X! Tandem (The GPM, thegpm.org; version CYCLONE 2010.12.01.1). SEQUEST was set to search the protein database downloaded from the UniProt protein database using the keyword Homo sapiens (downloaded 15 April 2014, total of 124,318 entries). The digestion enzyme was assumed to be trypsin. X! Tandem was set to search a subset of the database also assuming trypsin as the digestion enzyme. SEQUEST and X! Tandem were searched with a fragment ion mass tolerance of 0.50 Da and a parent ion tolerance of 1.00 Da. Scaffold (Version Scaffold_4.4.1.1; Proteome Software Inc., Portland, OR, USA) was used to validate MS/MS based peptide and protein identifications.

Statistical analysis

Data were shown as values (mean \pm standard deviation) and analyzed by ANOVA with Tukey's range-test or two-tailed unpaired Student's *t*-test to determine the significance of difference between groups using GraphPad Prism version 7. The *p*-values less than 0.05 were considered statistically significant.

Acknowledgements

This work was supported by Basic Science Research Program through the National Research Foundation of Korea (NRF) funded by the Ministry of Science, ICT & Future Planning (NRF-2018M3A9C8020027 and NRF-2017R1A2B3005015), the Tumor Microenvironment GCRC (2011-0030001), and the Medicinal Bioconvergence Research Center (NRF-2013M3A6A4044019) to J.W.L.

Author details

¹Department of Pharmacy, Research Institute of Pharmaceutical Sciences, College of Pharmacy, Seoul National University, Seoul 08826, Republic of Korea. ²Interdisciplinary Program in Genetic Engineering, Seoul National University, Seoul 08826, Republic of Korea. ³Systems Biotechnology Research Center, Korea Institute of Science and Technology (KIST), Gangneung-si, Gangwon-do 25451, Republic of Korea. ⁴Institute of Medical Science, Department of Biochemistry, School of Medicine, Jeju National University, Jeju 63243, Republic of Korea

Conflict of interest

The authors declare that they have no conflict of interest.

Publisher's note

Springer Nature remains neutral with regard to jurisdictional claims in published maps and institutional affiliations.

Supplementary Information accompanies this paper at (<https://doi.org/10.1038/s41419-019-1878-5>).

Received: 4 May 2019 Revised: 14 August 2019 Accepted: 26 August 2019
Published online: 09 September 2019

References

- Hewlett, J. C., Kropski, J. A. & Blackwell, T. S. Idiopathic pulmonary fibrosis: epithelial-mesenchymal interactions and emerging therapeutic targets. *Matrix Biol.* **71–72**, 112–127 (2018).
- Phan, S. H. Genesis of the myofibroblast in lung injury and fibrosis. *Proc. Am. Thorac. Soc.* **9**, 148–152 (2012).
- Sheppard, D. Epithelial-mesenchymal interactions in fibrosis and repair. Transforming growth factor-beta activation by epithelial cells and fibroblasts. *Ann. Am. Thorac. Soc.* **12**(Suppl 1), S21–S23 (2015).
- Misharin, A. V. & Budinger, G. R. S. Targeting the myofibroblast in pulmonary fibrosis. *Am. J. Respir. Crit. Care Med.* **198**, 834–835 (2018).
- Richter, K. & Kietzmann, T. Reactive oxygen species and fibrosis: further evidence of a significant liaison. *Cell Tissue Res.* **365**, 591–605 (2016).
- Jain, M. et al. Mitochondrial reactive oxygen species regulate transforming growth factor-beta signaling. *J. Biol. Chem.* **288**, 770–777 (2013).
- Bhakta-Guha, D. & Efferth, T. Hormesis: decoding two sides of the same coin. *Pharm. (Basel)* **8**, 865–883 (2015).
- Walraven, M. & Hinz, B. Therapeutic approaches to control tissue repair and fibrosis: extracellular matrix as a game changer. *Matrix Biol.* **71–72**, 205–224 (2018).
- Zhou, Y. et al. Extracellular matrix in lung development, homeostasis and disease. *Matrix Biol.* **73**, 77–104 (2018).
- Hogan, B. L. et al. Repair and regeneration of the respiratory system: complexity, plasticity, and mechanisms of lung stem cell function. *Cell Stem Cell* **15**, 123–138 (2014).
- Gonzalez-Gonzalez, F. J., Chandel, N. S., Jain, M. & Budinger, G. R. S. Reactive oxygen species as signaling molecules in the development of lung fibrosis. *Transl. Res.* **190**, 61–68 (2017).
- Lee, J. W. Transmembrane 4 L six family member 5 (TM4SF5)-mediated epithelial-mesenchymal transition in liver diseases. *Int. Rev. Cell Mol. Biol.* **319**, 141–163 (2015).
- Kim, H. J. et al. Dynamic and coordinated single-molecular interactions at TM4SF5-enriched microdomains guide invasive behaviors in 2- and 3-dimensional environments. *FASEB J.* **31**, 1461–1481 (2017).
- Kang, M. et al. Correlations between Transmembrane 4 L6 family member 5 (TM4SF5), CD151, and CD63 in liver fibrotic phenotypes and hepatic migration and invasive capacities. *PLoS ONE* **9**, e102817 (2014).
- Kang, M. et al. Antagonistic regulation of transmembrane 4 L6 family member 5 attenuates fibrotic phenotypes in CCl(4)-treated mice. *FEBS J.* **279**, 625–635 (2012).
- Lee, S. A. et al. Tetraspanin TM4SF5 mediates loss of contact inhibition through epithelial-mesenchymal transition in human hepatocarcinoma. *J. Clin. Invest.* **118**, 1354–1366 (2008).
- Lee, D. et al. Interaction of tetraspan (in) TM4SF5 with CD44 promotes self-renewal and circulating capacities of hepatocarcinoma cells. *Hepatology* **61**, 1978–1997 (2015).
- Prochazka, L., Tesarik, R. & Turanek, J. Regulation of alternative splicing of CD44 in cancer. *Cell Signal* **26**, 2234–2239 (2014).
- Koppula, P., Zhang, Y., Zhuang, L. & Gan, B. Amino acid transporter SLC7A11/xCT at the crossroads of regulating redox homeostasis and nutrient dependency of cancer. *Cancer Commun. (Lond.)* **38**, 12 (2018).
- Schulze-Osthoff, K., Beyaert, R., Vandevoorde, V., Haegeman, G. & Fiers, W. Depletion of the mitochondrial electron transport abrogates the cytotoxic and gene-inductive effects of TNF. *EMBO J.* **12**, 3095–3104 (1993).
- Lee, S. A. et al. Blockade of four-transmembrane L6 family member 5 (TM4SF5)-mediated tumorigenicity in hepatocytes by a synthetic chalcone derivative. *Hepatology* **49**, 1316–1325 (2009).
- Bansal, A. & Simon, M. C. Glutathione metabolism in cancer progression and treatment resistance. *J. Cell Biol.* **217**, 2291–2298 (2018).
- Dittmar, K. A. et al. Genome-wide determination of a broad ESRP-regulated posttranscriptional network by high-throughput sequencing. *Mol. Cell Biol.* **32**, 1468–1482 (2012).
- Lee, M. S., Kim, H. P., Kim, T. Y. & Lee, J. W. Gefitinib resistance of cancer cells correlated with TM4SF5-mediated epithelial-mesenchymal transition. *Biochim. Biophys. Acta* **1823**, 514–523 (2012).
- Choi, J. et al. Bidirectional signaling between TM4SF5 and IGF1R promotes resistance to EGFR kinase inhibitors. *Lung Cancer* **90**, 22–31 (2015).

26. Schieber, M. & Chandel, N. S. ROS function in redox signaling and oxidative stress. *Curr. Biol.* **24**, R453–R462 (2014).
27. Ishimoto, T. et al. CD44 variant regulates redox status in cancer cells by stabilizing the xCT subunit of system xc(-) and thereby promotes tumor growth. *Cancer Cell* **19**, 387–400 (2011).
28. Lee, J. W. TM4SF5-mediated protein-protein networks and tumorigenic roles. *BMB Rep.* **47**, 483–487 (2014).
29. Kim, S. et al. CD133-induced TM4SF5 expression promotes sphere growth via recruitment and blocking of protein tyrosine phosphatase receptor type F (PTPRF). *Cancer Lett.* **438**, 219–231 (2018).